Cellulose-Inorganic Hybrids of Strongly Reduced Thermal Conductivity

Panagiotis Spiliopoulos
Aalto University
Marie Gestranius
VTT Technical Research Centre of Finland Ltd.
Chao Zhang
University of Helsinki
Ramin Ghiyasi
Aalto University
John Tomko
University of Virginia
Kai Arstila
University of Jyväskylä
Matti Putkonen
University of Helsinki
Patrick E. Hopkins
University of Virginia
Maarit Karppinen
Aalto University
Tekla Tammelin
VTT Technical Research Centre of Finland Ltd.
Eero Kontturi (eero.kontturi@aalto.fi)
Aalto University https://orcid.org/0000-0003-1690-5288

Research Article

Keywords: cellulose nanocrystals, zinc oxide, hybrids, thermal conductivity, aluminum doping

Posted Date: June 21st, 2021

DOI: https://doi.org/10.21203/rs.3.rs-632419/v1

Abstract

The employment of atomic layer deposition and spin coating techniques for preparing inorganic-organic hybrid multilayer structures of alternating ZnO-CNC layers was explored in this study. Helium ion microscopy and X-ray reflectivity showed the superlattice formation for the nanolaminate structures and atomic force microscopy established the efficient control of the CNCs surface coverage on the Al-doped ZnO by manipulating the concentration of the spin coating solution. Thickness characterization of the hybrid structures was performed via both ellipsometry and X-ray reflectivity and the thermal conductivity was examined by time domain thermoreflectance technique. It appears that even the incorporation of a limited amount of CNCs between the ZnO laminates strongly suppresses the thermal conductivity. Even small, submonolayer amounts of CNCs worked as a more efficient insulating material than hydroquinone or cellulose nanofibers which have been employed in previous studies.

Introduction

Hybrids of inorganic-organic materials are expected to hold a pivotal role in future research topics, since the structural idea beyond them focuses on combining the desired properties out of each component. For example, organic layers sandwiched between inorganic layers can contribute to the harvesting of thermoelectric energy in thin film structures by decreasing the thermal conductivity of the material, without negative influence on the electrical properties (Wan et al. 2015; Wan et al. 2017). However, their efficient fabrication in a single pattern still exhibits a number of challenges. Inorganic thin film production by atomic layer deposition (ALD) has during recent decades developed into an industrial coating method, while still retaining its position as an indispensable method for deposition of thin inorganic layers in research context due to the numerous permutations of elements. More recently, research on molecular layer deposition (MLD), in which small bifunctional organic molecules in the form of precursors can be deposited in a similar manner as in ALD, has been progressing. The combination of these two methods allows the production of nanoscale organic-inorganic hybrid superlattices with molecular control of the layer thicknesses (Tynell et al. 2014; Khayyami et al. 2019). Although combined ALD and MLD is superior in control of the superlattice structure, the approach is still constrained by the limited selection of MLD precursors. Alternating inorganic-organic superlattice thin films with strongly reduced thermal conductivity have previously also been made from larger organic particles, namely nanocellulose, in which alternating layers have been produced by ALD deposition of ZnO and dip coating (Jin et al. 2017). In this paper, we want to refine the approach further by utilizing spin coating of highly specific and well-defined nanocellulose layers interspaced with ALD-deposited ZnO layers.

As a semiconductor, ZnO possesses many positive attributes for thermoelectric energy harvesting, such as high electrical conductivity and high Seebeck coefficient (Hahn et al. 1951). Moreover, ZnO is nontoxic, inexpensive and a commonly used material deposited with ALD, its behavior is well known and predictable as it is considered an ALD protype material (Tynell et al. 2014; Yousfi et al. 2000). The high thermoconductivity of ZnO is, however, a challenge in thermoelectric applications; hence, introduction of organic materials with low thermoconductivity has been suggested to reduce it (Jin et al.

2017). Aluminum doping of ZnO, increases the conductivity, but has also been introduced as a method to decrease the thermal conductivity of nanocomposites (Jood et al. 2011) and a moderate Al-doping of the ZnO has other advantages as it decreases the roughness of ALD-grown films (Banerjee et al. 2010).

Assuming their form as nanosized, anisotropic particles extracted from natural fibers, nanocellulose has been topical for the past 10-15 years in materials research that has capitalized on its advanced mechanical properties (Aitomäki et al. 2014), high surface area (Phanthong et al. 2018), low toxicity (Endes et al. 2016) and low thermal conductivity (Hori et al. 2005; Uetani et al. 2017; Wicklein et al. 2015) among others. While the bulk of materials applications have centered around nanocomposites (Kargazadeh et.al 2017), membranes (Abraham et al. 2013) or drug delivery systems (Moritz et al. 2014; Liu et al. 2018), energy related applications, such as supercapacitors (Zu et al. 2016; Jose et al. 2019) have recently gained ground. In addition, inclusion of nanocellulose in thin film structures has been translated into solutions for sensors in particular (Mangayil et al. 2017; Nguyen et al. 2019). In our group, we have optimized the low temperature ALD multilayer deposition process on nanocellulose for the control over oxygen and water vapor transmission rates (Putkonen et al. 2017). The employment of nanocellulose for fabrication of energy-related hybrid inorganic-organic systems, however, still exhibits plenty of space to be explored.

Nanocelluloses come in a variety regarding their aspect ratio, shape, surface charge and crystallinity. CNFs correspond to mechanically isolated microfibrils out of the fiber bundle (Kim et al. 2015), while CNCs refer to much shorter rigid, rod-like particles (Dufresne et al. 2019). CNCs consist of highly crystalline cellulose, extracted from cellulosic fibers via hydrolysis procedure (Pääkkönen et al. 2019; Chen et al. 2015). As a result, it exhibits higher chemical homogeneity than CNFs because the hemicellulose with CNCs has been mostly degraded and removed upon the hydrolysis (Spiliopoulos et al. 2021; Wyman et al. 2005; Gao et al. 2014). In addition, their employment carries another significant advantage: CNCs can be coated as well-defined submonolayers and thicker films on metal oxide surfaces, with efficient control over the surface coverage by simply altering the solution concentration in spin coating (Kontturi et al. 2007). Previous work by our group has focused on the ZnO thermal conductivity reduction by the incorporation of TEMPO oxidized cellulose nanofibers (TOCNFs) between the ZnO layers, resulting in hybrid superlattice structures with potential as possible thermoelectric materials (Jin et al. 2017). However, because the CNF coverage is difficult to control, the effect was not quantified to the organic/inorganic component ratio.

In this study, a simple and easily reproducible experimental protocol was applied, aiming at the incorporation of cellulose nanocrystals (CNCs) between ZnO to construct hybrid nanolaminates. To investigate the efficiency of our protocol, we resorted to a sizeable variety of characterization techniques: helium ion microscopy (HIM) and X-ray reflectivity (XRR) for the superlattice structure, atomic force microscopy (AFM) for the layer morphology, ellipsometry and XRR for the layer thickness, and time domain thermoreflectance (TDTR) for thermal conductivity of the resulting ultrathin films. Figure 1 shows the construction of hybrid superlattice structures involving Al-doped ZnO nanolaminates interspaced with CNCs at different surface coverage. Organic and inorganic layers were prepared by spin

coating and ALD, respectively. Spin-coating is a fast and reproducible technique for cellulose films fabrication (Kontturi et al. 2003) whereas ALD is a well-established, efficient method for facilitating inorganic thin films, like ZnO (Singh et al. 2014; Boyadjiev et al. 2016). Herein, a significant reduction in thermal conductivity was demonstrated, even by the incorporation of very limited amounts of CNCs in the superlattice.

Experimental

CNC preparation

Commercial bacterial cellulose (BC, Chaokoh Nata De Coco, Theppadungporn Coconut Co., Ltd, Thailand) was used as the raw material of CNCs. The BC cubes were stored in coconut gel and washed thoroughly with pure water followed by alkali extraction with 0.1 M NaOH (3 hours, 85 °C) for purification. Finally, the BC cubes were once more washed thoroughly with pure water. The extracted product was freeze dried (Edwards Micro Modulyo Freeze Dryer, Crawley, England) with the noted pre-treatments to dry matter content > 90 %. The HCl gas hydrolysis of the freeze-dried material down to LODP (Leveling-off Degree of Polymerization) took place in a custom-built reactor (Pääkkönen et al. 2018) at 1.0 bar of pressure for 21 hours, followed by degassing and extensive washing with milli-pore water. TEMPO-mediated oxidation was performed in a Büchi reactor (volume 1.6 dm^3) as described by Pääkkönen et al. (2019) and the charge-carboxylate content of the hydrolyzed and TEMPO-oxidized BC was determined by conductometric titration (SCAN-CM 65:02) using Metrohm 751 GPD Titrino automatic titrator and Tiamo 1.2.1. Software. The charge content was calculated to 1.0 mmol/g, arising exclusively from the carboxylate amount of the sample. The average dimensions of the BC-CNCs were extracted from atomic force microscopy (AFM) and transmission electron microscopy (TEM) measurements and found to be 170 nm in length and 10 – 15 nm in diameter (Pääkkönen et al. 2019).

Hybrid inorganic-organic thin films preparation

The hybrid superlattice structures were fabricated by alternation of ALD depositions of Al-doped ZnO layers and spin coating of cellulose nanocrystals (CNCs) dispersions of three different concentrations: 25, 100 and 250 mg dm^{-3}. Single side polished Si wafers of P-type doped with boron and with the orientation (100) produced by Okmetic were cut with a dicing saw (Disco Corporation, Tokyo, Japan) to 1 × 1 cm^2 substrates. Prior to use, the substrates were cleaned by soaking for 5 min in 2.5 M NaOH, followed by rinsing in Milli-Q water and drying with N_2 gas. The substrates were further coated with 5 layers of ZnO separated by 4 layers of CNCs (Figure 1). The layered structures were additionally prepared on 1 × 1 cm^2 single-side polished sapphire substrates (AdValue Technlogy, Tucson), following exactly the same procedure. The process was repeated for all CNC concentrations. The ALD deposition of ZnO was performed at 90 ^oC in a Picosun™ R-200 reactor (Picosun Oy, Espoo, Finland). The operating pressure of the reaction chamber was around 10 mbar. Inert nitrogen gas with a purity of 99.999% was used as the carrier and purge gas. Diethyl zinc (DEZ, ≥52 wt. % Zn basis) purchased from Sigma-Aldrich) and distilled (DI) water were used as precursors for the deposition of ZnO. The pulse time of 0.2 s and purge

time of 7.0 s were used for both precursors. ZnO doping was carried out by Al_2O_3 via the use of trimethyl aluminum (TMA) and H_2O as precursors with the pulse and purge times of 0.3 and 10.0 s for both precursors. The growth rates of binary materials for ZnO and Al_2O_3 thin films were around 0.2 nm/cycle and 0.1 nm/cycle, respectively. Al doping content in ZnO films was controlled by the so-called supercycle ALD, i.e., a single TMA- H_2O cycle was inserted after a defined number of DEZ-H_2O water cycles (Banerjee et al . 2010). The ALD supercycle of 13 × [10 × (DEZ + H_2O) + 1 × (TMA + H_2O)] was used to deposit the ZnO thin films with a target thickness of around 20 nm and the estimated Al doping ratio of 5%. Notably, in order to attain a uniform growth of ZnO thin films on the nanocellulose coating, 3 cycles of TMA-H_2O ALD were conducted before the ZnO ALD supercycles, as proposed by Baji et al. (2012). Spin coating of CNCs took place via a P-6000 spin coater (Speedline Technologies, Inc.) at 4,000 rpm for 90 seconds.

Helium ion microscopy (HIM)

For HIM imaging of the thin film hybrid structures, reference samples of tin on carbon and gold on silicon were employed. The hybrid films were placed on 45^o stubs and imaged from flat cleaved edge and from a scratch through a diamond pen. The imaging was performed via a Carl Zeiss Orion NanoFab instrument, utilizing a 35 keV helium beam. The working distance varied between 7-8 mm and the sample position alternated between 45^o and 90^o relative to the beam. The beam current was 0.15 – 0.20 pA and the image size 2048 × 2048 pixels. The dwell time was set at 10.0 μs and the line averaging at 4. Charge neutralization (flood gun) was not used. The pressure in the measurement chamber was 1.7 × 10-7 Torr. Finally, all images were post-processed by level adjustment and gamma.

Atomic force microscopy (AFM)

The hybrid films were examined after each coating layer by an AFM Multimode 8 microscope (J scanner) from Bruker AXS Inc. (Madison, Wisconsin USA) for all concentrations of CNCs. The imaging was done with Ultrasharp μmasch silicon tips (HQ: NSC15/Al BS, Tallin, Estonia) via tapping mode. The typical force constant was 40 N/m and the resonance frequency was 325 kHz. Third order flattening and 3D image generation was performed in Nanoscope Analysis 1.5 software. The analysis of film images and the surface coverage estimation were subsequently done by ImageJ 1.52a (Wayne Rasband, National Institute of Health, USA) software.

Ellipsometry characterization

Hybrid films thickness values were measured by a FS-1 multiwavelength ellipsometer (Film Sense), after each ZnO coating layer. Wavelengths of 465, 525, 590 and 635 nm were used to acquire the data. The Cauchy model was used for modeling the optical constants of the ZnO films.

X-Ray reflectivity (XRR)

The multilayer superlattice formation was analyzed by an X'pert Reflectivity v. 1.3 form PANalytical. The patterns were fitted by structural modelling. For the hybrid superlattice films, the initial fitting model –

from bottom to top, respectively – included the following layers: Si substrate, SiO_2, ZnO layer (10% Al_2O_3), corresponding number of cellulose and ZnO (10% Al_2O_3) layers, ending up with Al_2O_3 and (H_2O+CO_2) on top. The experimental data were fitted using Reflex v44 (Vignaud et al. 2019). During the fitting process all factors including thickness, density and roughness as well as instrumental factors were modified for fitting to the experimental pattern. The thickness values were confirmed by Fourier method to improve their reliability. Analytical details on the fitting procedure are described in the Supplementary Information (S5).

Time-domain thermoreflectance (TDTR)

The cross-plane thermal conductivity of the hybrid films was determined with the time-domain thermoreflectance (TDTR) technique at room temperature. Hybrid films of 5 inorganic (ZnO) and 4 organic (CNCs) layers were prepared on sapphire substrates and employed for the measurements. The thermal conductivity of the samples was obtained by fitting of the experimental 'cooling curve' with a multilayer heat flow model (Cahil et al. 2004), where the thermo physical properties of the substrate and a metal transducer layer (80 nm Al), as well as the thermal resistance of their respective interfaces, are accounted for. In principle, the heat flow model takes under consideration: (i) an Al film transducer (necessary for TDTR measurements to relate the measured reflectivity to temperature), (ii) the ZnO/CNC hybrid film, (iii) the sapphire substrate. The pertinent details of the experimental setup and the analysis procedure to determine the thermal conductivity of the hybrid thin films can be found by Giri et al. (2016a, b)

Results And Discussion

The formation of a superlattice structure was confirmed using several different methods. Figure 2 shows the HIM images visualizing the multilayered (N=9) hybrid structure of the sample cross sections. The use of HIM allowed high resolution imaging clearly showing the inorganic-organic layer alteration, making it evident that the formation of ZnO/CNC hybrid layered structures had been successful.

Alongside the HIM images, a clear sign of the superlattice structure was provided by the XRR data, strengthening the validity of the concept. The alternation of the superlattice peaks as the coating procedure is advancing is clearly visible through the reflection pattern of Figure 3.

The formation of additional intermediate fringes between the superlattice peaks is notable as the N number is increasing (Figure 3). For the 250 mg dm^{-3} concentration hybrids these fringes appear broader throughout all the (N) layers, something that could be attributed to the full coverage provided by the CNC layers on the ZnO (see, Figure 4 – AFM analysis and Table 1). In principle, the intercalating full-coverage CNC layers between the inorganic ones result in efficient separation of the superlattice peaks, while the presence of lower coverage CNC layers (25 and 100 mg dm^{-3}) appears not to lead to efficient ZnO layer separation. As a result, the XRR patterns from the films with 25 and 100 mg dm^{-3} CNC concentrations appear not as distinct as those from the films with 250 mg dm^{-3} CNC concentration. This occurs simply

because the ZnO/CNC interfaces for the 25 and 100 mg dm^{-3} hybrid films are not perfectly defined, due to the lower coverage at the smaller CNC concentrations – an explanation which is also supported by our previous study (Jin et al. 2017).

The Si-wafers substrates were efficiently coated with Al-doped ZnO (N=1) whose morphology and surface coverage is demonstrated in the Supplementary Information (Figure S1). For the following layers, AFM height images after layers N=2, 3, 9 are presented in Figure 4 and corresponding AFM height images for the remaining deposition steps are available in the Supplementary Information (Figure S2).

As observed, CNCs submonolayer formation takes place for ZnO/CNC (N=2, c=25 mg dm^{-3}) and ZnO/CNC (N=2, c=100 mg dm^{-3}) hybrids, while only for ZnO/CNC (N=2, c=250 mg dm^{-3}) full coverage is achieved (Figure 4 a-c, Supporting Information Figure S3). In addition, the ZnO deposition on CNCs induces a morphological alteration especially on ZnO/CNC (N=3, c=25 mg dm^{-3}) and ZnO/CNC (N=9, c=25 mg dm^{-3}) films, as well as through the intermediate stages (see also Supporting Information Figure S2) where the consecutive coating layers result in visible roughness increase in the AFM images. In fact, the lower CNC coverage of ZnO/CNC (N=2, c=25 mg dm^{-3}) and ZnO/CNC (N=2, c=100 mg dm^{-3}) enables the visualization of the coating effect via comparison with the ZnO/CNC (N=9, c=25 mg dm^{-3}) and ZnO/CNC (N=9, c=100 mg dm^{-3}) images. It should also be mentioned that the lower roughness indicated for the 25 mg/l concentration hybrids from the XRR analysis (Fig. 3), appears to be beneficial for observing the coating effect through the AFM images, in contrast with the increased roughness indicated for the 250 mg/l hybrids.

Table 1 demonstrates the surface coverage (SC) CNC values for the 3 different concentrations used as well as the surface roughness values, as calculated from the AFM data in Figure 4. In summary, the HIM, XRR and AFM measurements have provided us with a clear evidence of the concept on the hybrid multilayered structure formation.

Ellipsometry measurements took place after every ZnO deposition to establish the thickness values of the hybrids. Figure 5 shows these values, together with those from the XRR characterization, demonstrating a good correlation between the two techniques for thickness measurements.

As expected, the addition of layers increases the overall hybrid film thickness linearly with the number of layers added. Additionally, a small effect of the CNC concentration on the overall hybrid film thickness was detected by ellipsometry in Figure 5a, as higher CNC concentrations resulted into thicker films. The XRR data did not detect these small variations caused by the CNC concentration, probably due to the film roughness (Table 1), so only an average value of 85 nm for N=9 CNC/ZnO samples is presented in Figure 5b. On the other hand, the XRR data enabled us to determine the individual CNC layer thicknesses in the hybrid films: this value was found to increase from 1.5 nm to 3.0 nm and finally to 3.5 nm with increasing CNC concentration from 25 to 100 and to 250 mg dm^{-3} respectively. Thickness measured by XRR and ellipsometry also correspond relatively well to thickness measurement from the HIM images as well, as presented in the Supplementary Information (Table S1). Image analysis from HIM images gave slightly

smaller thickness estimates, in the range of -4 to -7 nm compared to ellipsometry, possibly due to the ultra-high vacuum the samples were subjected to in the HIM. The minor variations in thickness – measured from several different locations of the N=9 hybrids with HIM – underline a uniform thickness throughout the sample and the repeatability of the layer build up process.

The thermal conductivity values obtained from the TDTR measurements are demonstrated in Figure 6. The entire N=9 samples for 25, 100 and 250 mg dm^{-3} CNC concentrations were examined and a comparison to hybrid samples with a different insulating component (hydroquinone and cellulose nanofibers) from previous studies (Tynell et al. 2014; Jin et al. 2017) is presented. A large reduction in the thermal conductivity takes places for all the ZnO/CNC samples not only compared to that of a ZnO film (Alvarez-Quintana et al. 2010) but also to the values of those previous studies.

Cellulose nanofibers (CNF) have been proved more efficient in reducing the thermal transport in ZnO films than hydroquinone (HQ), but the incorporation of CNC layers between the ZnO laminates resulted in even lower thermal conductivity than CNF, as demonstrated in Figure 6. Herein, the comparison between the thermal conductivities of ZnO/CNF and ZnO/CNC hybrids is relevant since all of them are composed of the same layer number (N=9). The ALD layers produced in this study are doped with aluminum, which is a known route to reduce the thermal conductivity of ZnO in bulk when compared to ZnO and $ZnAl_2O_4$ nanocomposites (Jood et al. 2011). However, the system differs highly from the one in this study, as it is disordered compared to this nanolaminate. It is also clear that the incorporation of different CNC concentrations has a small but clear effect on the thermal conductivity value. We attribute this to the increasing CNC layer thickness (1.5, 3.0 and 3.5 nm) with increasing CNC concentration (25, 100 and 250 mg dm^{-3}), in agreement with the previous studies (Jin et al. 2017, Ghiyasi et al. 2020, 2021) which have also pointed out the beneficial role of the increased organic layer thickness in depressing the thermal conductivity of the hybrid.

It is apparent that the more elaborate and reproducible technique of spin coating in this work facilitates more defined cellulose layers than the simple dipping of the substrate in the CNF suspension that was performed by Jin et al. (2017). Controlled, homogeneously spread layers of CNCs lead to a more efficient scattering of phonons, thereby minimizing the cross-plane thermal conduction. It would be reasonable to assume that increasing the CNC concentration – and as a result the CNC surface coverage and finally the thickness of the organic component – would diminish the phonon propagation even further, but this was not the case. In fact, an increase of the CNC concentration (i.e., the thickness of the CNC layers) has a relatively mild effect on the thermal conductivity as an increase in concentration to 100 and 250 mg/dm^{-3} reduced the thermal conductivity 11% and 25% respectively compared with the 25 mg/dm^{-3} case, as calculated by the values of Figure 6 (see Supporting Information, Figure S4). It appears that even the incorporation of a limited amount of CNCs through the ZnO laminates can induce a significant reduction in the thermal conductivity, while the formation of a full-coverage CNC layer is not a requirement for achieving this reduction.

Conclusions

Layered hybrid ZnO/CNC films were prepared by a combination of ALD and spin-coating techniques. HIM, XRR and AFM data confirmed the presence of a multilayered structure, constructed of discrete, alternating layers of ZnO and CNC, amounting to superlattice structures. TDTR examined the hybrids cross plane thermal conductivity, establishing a large reduction after the CNC incorporation. It appears that even the formation of a CNC submonolayer, without ensuring full coverage on the ZnO wafers, can result in efficient phonons scattering through the cross plane, while the intercalation of thicker CNC layers causes a mild additional decrease in the thermal conductivity of the hybrid film.

Declarations

Funding

PS and MG were funded by Academy of Finland (grants no. 300364 and 300367). MK and RG received funding from European Union's Horizon 2020 research and innovation program under the Marie Sklodowska-Curie grant agreement (No. 765378), the Academy of Finland (Profi 3) and the use of RawMatters Finland Infrastructure (RAMI) at Aalto University. M.P received funding from the Academy of Finland by the profiling action on Matter and Materials, grant no. 318913. The work is a part of FinnCERES Materials Bioeconomy Ecosystem.

Conflicts of interest/Competing interests

Not applicable.

Availability of data and material

Not applicable.

Authors' contributions

Not applicable.

Additional declarations for articles in life science journals that report the results of studies involving humans and/or animals

Not applicable.

Ethics approval

There are no ethical issues to consider.

Consent to participate

All authors have participated in the writing of the manuscript and given their consent to submit the manuscript.

Consent for publication

All authors consent to the publication of the manuscript.

Acknowledgements

PS and MG would like to acknowledge Academy of Finland (grants no. 300364 and 300367) for the financial support. MK and RG would like to acknowledge the Europian Union's Horizon 2020 research and innovation program under the Marie Sklodowska-Curie grant agreement (No. 765378), the Academy of Finland (Profi 3) and the use of RawMatters Finland Infrastructure (RAMI) at Aalto University. M.P acknowledges funding from Academy of Finland by the profiling action on Matter and Materials, grant no. 318913. The work is a part of FinnCERES Materials Bioeconomy Ecosystem.

References

1. Abraham E, Thomas MS, John C, Pothen LA, Shoseyov O. Thomas S (2013) Green nanocomposites of natural rubber/nanocellulose: membrane transport, rheological and thermal degradation characterisations. Ind Crops Prod 51:415-424. https://doi.org/10.1016/j.indcrop.2013.09.022
2. Aitomäki Y, Oksman K (2014) Reinforcing efficiency of nanocellulose in polymers. React Funct Polym 85:151-156. https://doi.org/10.1016/j.reactfunctpolym.2014.08.010
3. Alvarez-Quintana, J, Martinez E, Pérez-Tijerina E, Pérez-García SA, Rodríguez-Viejo J (2010) Temperature dependent thermal conductivity of polycrystalline ZnO films. J Appl Phys 107:063713. https://doi.org/10.1063/1.3330755
4. Baji Z, Lábadi Z, Horváth ZE et al (2012) Nucleation and growth modes of ALD ZnO. Cryst Growth Des 12:5615-5620. https://doi.org/10.1021/cg301129v
5. Banerjee P, Lee WJ, Bae KR, Lee SB, Rublof GW (2010) Structural, electrical, and optical properties of atomic layer deposition Al-doped ZnO films. J Appl Phys 108: 043504. https://doi.org/10.1063/1.3466987
6. Boyadjiev SI, Georgieva V, Yordanov R, Raicheva Z, Szilágyi IM (2016) Preparation and characterization of ALD deposited ZnO thin films studied for gas sensors. Appl Surf Sci 387: 1230-1235. https://doi.org/10.1016/j.apsusc.2016.06.007
7. Cahill DG (2004) Analysis of heat flow in layered structures for time-domain thermoreflectance. Rev Sci Instrum 75:5119-5122. https://doi.org/10.1063/1.1819431
8. Chen L, Wang Q, Hirth K, Baez K, Argarwal UP, Zhu JY (2015) Tailoring the yield and characteristics of wood cellulose nanocrystals (CNC) using concentrated acid hydrolysis. Cellulose 22:1753-1762. http://dx.doi.org/10.1007/s10570-015-0615-1

9. Dufresne A (2019) Nanocellulose processing properties and potential applications. Curr For Rep 5:76-89. https://doi.org/10.1007/s40725-019-00088-1
10. Endes C, Camarero-Espinosa S, Mueller S et al (2016) A critical review of the current knowledge regarding the biological impact of nanocellulose. J Nanobiotechnology 14: 1-14. DOI:10.1186/s12951-016-0230-9
11. Gao X, Rajeev K, Wyman CE (2014) Fast hemicellulose quantification via a simple one-step acid hydrolysis. Biotechnol Bioeng 111:1088-1096. http://dx.doi.org/10.1002/bit.25174
12. Ghiyasi R, Girish C.T, Karppinen M (2020) Organic-Component Dependent Crystal Orientation and Electrical Transport Properties in ALD/MLD Grown ZnO–Organic Superlattices. Phys Chem C 124: 13765-13770. https://doi.org/10.1021/acs.jpcc.0c03053
13. Ghiyasi R, Milich M, Tomko J, Hopkins PE, Karpinnen M (2021) Organic component dependent thermal conductivity reduction in ALD/MLD grown ZnO: organic superlattice thin films. Appl Phys Lett 118:211903. https://doi.org/10.1063/5.0052450
14. Giri A, Niemelä JP, Szwejkowski CJ, Karppinen M, Hopkins PE (2016) Reduction in thermal conductivity and tunable heat capacity of inorganic/organic hybrid superlattices. Phys Rev B 93:115-310. https://doi.org/10.1103/PhysRevB.93.115310
15. Giri A, Niemelä JP, Tynell T, Gaskins JT, Donovan BF, Karppinen M, Hopkins PE (2016) Heat-transport mechanisms in molecular building blocks of inorganic/organic hybrid superlattices. Phys Rev B 93: 115310. https://doi.org/10.1103/PhysRevB.93.11531
16. Hahn EE (1951) Some electrical properties of zinc oxide semiconductor. J Appl Phys22:855-863. https://doi.org/10.1063/1.1700063
17. Hori R, Wada M (2005) The thermal expansion of wood cellulose crystals. Cellulose 12:479-484. https://doi.org/10.1007/s10570-005-5967-5
18. Jin H, Marin G, Giri A, Tynell T, Gestranius M, Wilson BP, Kontturi E, Tammelin T, Hopkins PE, Karppinen M (2017) Strongly reduced thermal conductivity in hybrid ZnO/nanocellulose thin films. J Mater Chem 52:6093-6099. https://doi.org/10.1007/s10853-017-0848-5
19. Jood P, Mehta RJ, Zhang Y et al (2011) Al-doped zinc oxide nanocomposites with enhanced thermoelectric properties. ACS Nano 11: 4337-4342. https://doi.org/10.1021/nl202439h
20. Jose J, Thomas V, Vinod V, Abraham R, Abraham S (2019) Nanocellulose based functional materials for supercapacitor applications. J Sci adv mater dev 4:333-340.
21. Zu G, Shen J, Zou L, Wang F, Wang X, Zhang Y, Yao X (2016) Nanocellulose-derived highly porous carbon aerogels for supercapacitors. Carbon 99:203-211. https://doi.org/10.1016/j.carbon.2015.11.079
22. Kargarzadeh H, Mariano M, Huang J, Lin N, Ahmad I, Dufresne A, Thomas S et al (2017) Recent developments on nanocellulose reinforced polymer nanocomposites: A review. Polymer 132: 368-393.
23. Khayyami A, Philip A, Karppinen M (2019) Atomic/Molecular layer deposited iron–azobenzene framework thin films or stimuli-induced gas molecule capture/release. Angew Chem Int Ed 58:13400-

13404. https://doi.org/10.1002/anie.201908164

24. Kim JH, Shim BS, Kim SH, et al (2015) Review of nanocellulose for sustainable future materials. Int J Precis Eng Manuf 2:197-213. https://doi.org/10.1007/s40684-015-0024-9
25. Kontturi E, Johansson LS, Kontturi KS, Ahonen P, Thüne PC, Laine J (2007) Cellulose nanocrystal submonolayers by spin coating. Langmuir 23: 9674-9680. https://doi.org/10.1021/la701262x
26. Kontturi E, Thüne PC, Niemantsverdriet JW (2003) Novel method for preparing cellulose model surfaces by spin coating. Polymer 44: 3621-3625.
27. Liu Y, Sui Y, Liu C, Liu C, Wu M, Li B, Li Y (2018) A physically crosslinked polydopamine/nanocellulose hydrogel as potential versatile vehicles for drug delivery and wound healing. Carbohydr Polym 188:27-36. https://doi.org/10.1016/j.carbpol.2018.01.093
28. Mangayil R, Rajala S, Pammo A, Sarlin E, Luo J, Santala V, Karp M, Tuukkanen S (2017) Engineering and characterization of bacterial nanocellulose films as low cost and flexible sensor material. ACS Appl Mater Interfaces 9:19048-19056. https://doi.org/10.1021/acsami.7b04927
29. Moritz S, Wiegand C, Wesarg F, Hessler N, Müller FA, Kralisch D, Hipler UC, Fischer D (2014) Active wound dressings based on bacterial nanocellulose as drug delivery system for octenidine. Int J Pharm 471:45-55. https://doi.org/10.1016/j.ijpharm.2014.04.062
30. Nguyen LH, Naficy S, Chandrawati R, Dehghani F (2019) Nanocellulose for sensing applications. Adv Mater Interfaces 6: 1900424. https://doi.org/10.1002/admi.201900424
31. Pääkkönen T, Spiliopoulos P, Knuts A, Nieminen K, Johansson LS, Enqvist E, Kontturi E (2018) From vapour to gas: optimising cellulose degradation with gaseous HCl. React Chem Eng 3: 312-318. https://doi.org/10.1039/C7RE00215G
32. Pääkkönen T, Spiliopoulos P, Nonappa, Kontturi KS, Penttilä P, Viljanen M, Svedström K, Kontturi E (2019) Sustainable high yield route to cellulose nanocrystals from bacterial cellulose. ACS Sustain Chem Eng 7:14384-14388. https://doi.org/10.1021/acssuschemeng.9b04005
33. Phanthong P, Reubroycharoen P, Hao X, Xu G, Abudula A, Guan G et al (2018) Nanocellulose: Extraction and application. Carbon Resour Convers 1:32-43. https://doi.org/10.1016/j.crcon.2018.05.004
34. Putkonen, M, Sippola, P, Svärd, L, Sajavaara, T, Vartiainen, J, Buchanan, I, Forsström, U, Simell, P, Tammelin, T (2017) Low-temperature atomic layer deposition of SiO2/Al2O3 multilayer structures constructed on self-standing films of cellulose nanofibrils Phil Trans R Soc A 376: 20170037. http://dx.doi.org/10.1098/rsta.2017.0037
35. Singh T, Lehnen T, Leuning T, Sahu D, Mathur S (2014) Thickness dependence of optoelectronic properties in ALD grown ZnO thin films. Appl Surf Sci 289:27-32. https://doi.org/10.1016/j.apsusc.2013.10.071
36. Spiliopoulos P, Spirk S, Pääkkönen T, Viljanen M, Svedström K, Pitkänen L, Awais M, Kontturi E (2021) Visualizing degradation of cellulose nanofibers by acid hydrolysis. Biomacromolecules 22:1399-1405. https://doi.org/10.1021/acs.biomac.0c01625

37. Tynell T, Giri A, Gaskins J, Hopkins PE, Mele P, Miyazaki K, Karppinen M (2014) Efficiently suppressed thermal conductivity in ZnO thin films via periodic introduction of organic layers. J Mater Chem A 2:12150-12152. https://doi.org/10.1039/C4TA02381A
38. Tynell T, Karppinen M (2014) Atomic layer deposition of ZnO: a review. Semicond Sci Technol 29:043001.
39. Uetani K, Hatori K (2017) Thermal conductivity analysis and applications of nanocellulose materials. Sci Technol Adv Mater 18: 877-892. https://doi.org/10.1080/14686996.2017.1390692
40. Vignaud G, Gibaud A (2019) REFLEX: a program for the analysis of specular X-ray and neutron reflectivity data. J Appl Cryst 52:201-213. https://doi.org/10.1107/S1600576718018186
41. Wan C, Gu X, Dang F et al (2015) Flexible n-type thermoelectric materials by organic intercalation of layered transition metal dichalcogenide TiS_2. Nat Mater 14: 622-627. http://dx.doi.org/10.1038/nmat4251
42. Wan C, Tian R, Kondou M, Yang R, Zong P, Koumoto K (2017) Ultrahigh thermoelectric power factor in flexible hybrid inorganic-organic superlattice. Nat Commun 8:1-9. DOI: 10.1038/s41467-017-01149-4
43. Wicklein B, Kocjan A, et al (2015) Thermally insulating and fire-retardant lightweight anisotropic foams based on nanocellulose and graphene oxide. Nat Nanotechnol 10:277-283. https://doi.org/10.1038/nnano.2014.248
44. Wyman CE, Decker SR, Himmel ME, Brady JW, Skopec CE, Viikari L (2005) Hydrolysis of cellulose and hemicellulose. Polysaccharides: Structural diversity and functional versatility 1023-1062.
45. Yousfi EB, Fouache J, Lincot D (2000) Study of atomic layer epitaxy of zinc oxide by in-situ quartz crystal microgravimetry Appl Surf Sci 153: 223-234. https://doi.org/10.1016/S0169-4332(99)00330-X

Tables

Table 1. Surface coverage (SC) values and roughness (root mean square) values for the ZnO/CNC (N=2, c=25 mg dm^{-3}), ZnO/CNC (N=2, c=100 mg dm^{-3}) and ZnO/CNC (N=2, c=250 mg dm^{-3}) hybrids, as calculated by image analysis from AFM data

ZnO/CNC sample	N=2, c= 25 mg dm^{-3}	N=2, c= 100 mg dm^{-3}	N=2, c= 250 mg dm^{-3}
CNC, SC %	12.3 ± 2.08	17.3 ± 0.57	100
Roughness (nm)	3.0	3.5	3.3

Figures

Figure 1

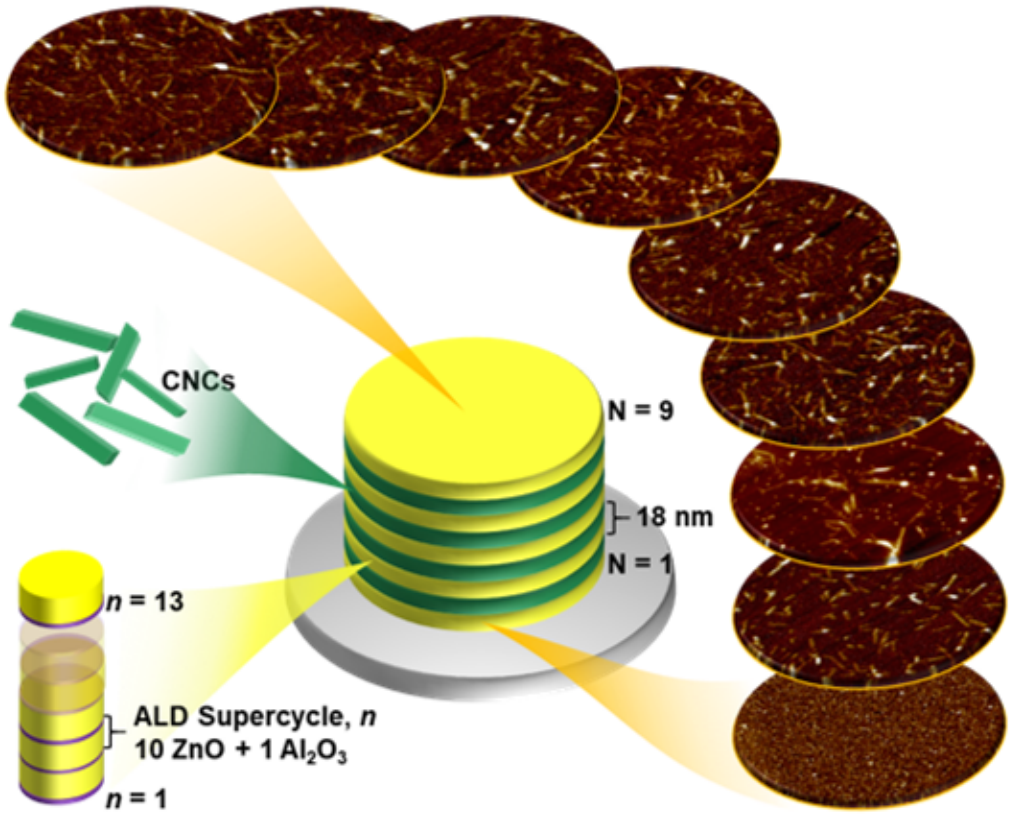

Figure 1

Hybrid superlattice thin-film structure, consisting of 5 Al-doped ZnO layers alternating with 4 CNC layers

Figure 2

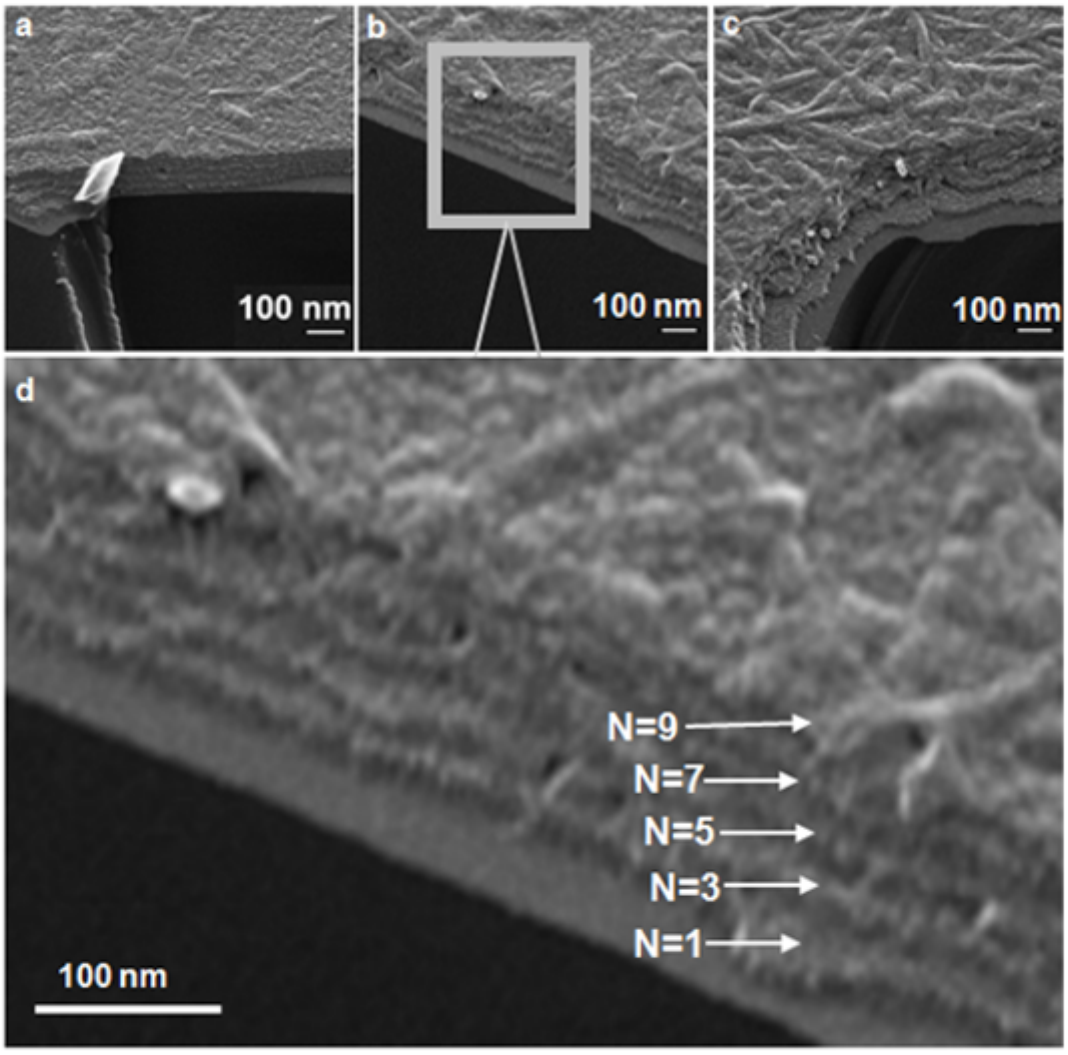

Figure 2

HIM images of the cross sections of (a) ZnO/CNC (N=9, c=25 mg dm-3), (b) ZnO/CNC (N=9, c=100 mg dm-3), (c) ZnO/CNC (N=9, c=250 mg dm-3) and (d) ZnO/CNC (N=9, c=100 mg dm-3) high resolution image

Figure 3

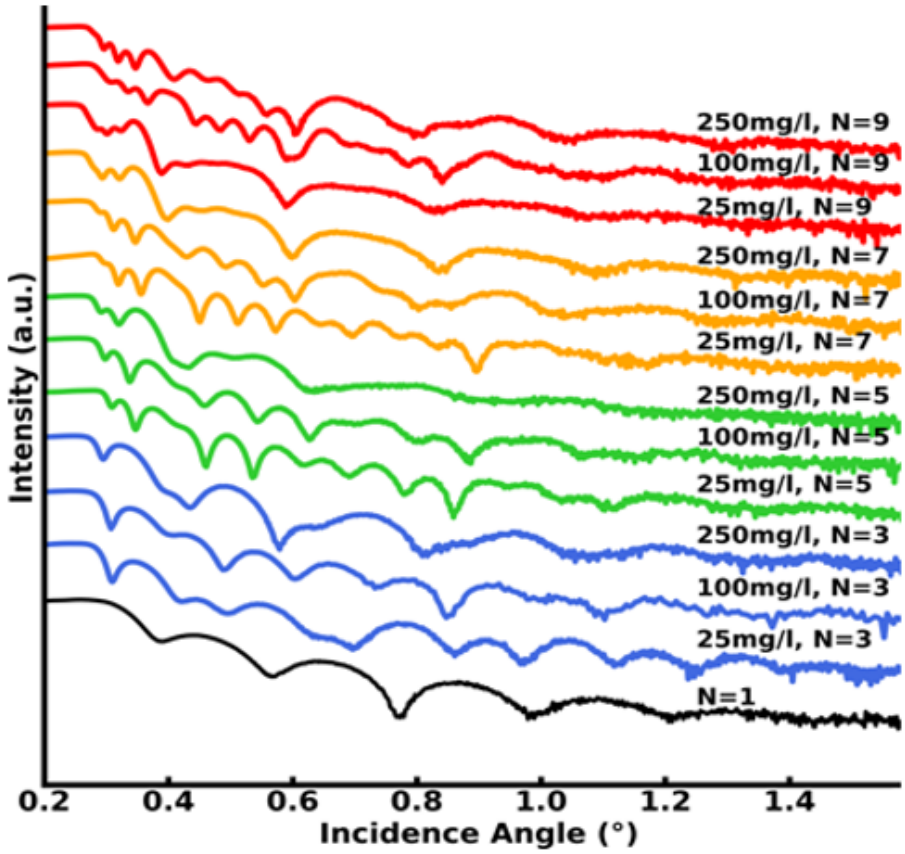

Figure 3

XRR patterns of the hybrid samples. N number denotes the coating layer sequence and each concentration is mentioned above the corresponding pattern.

Figure 4

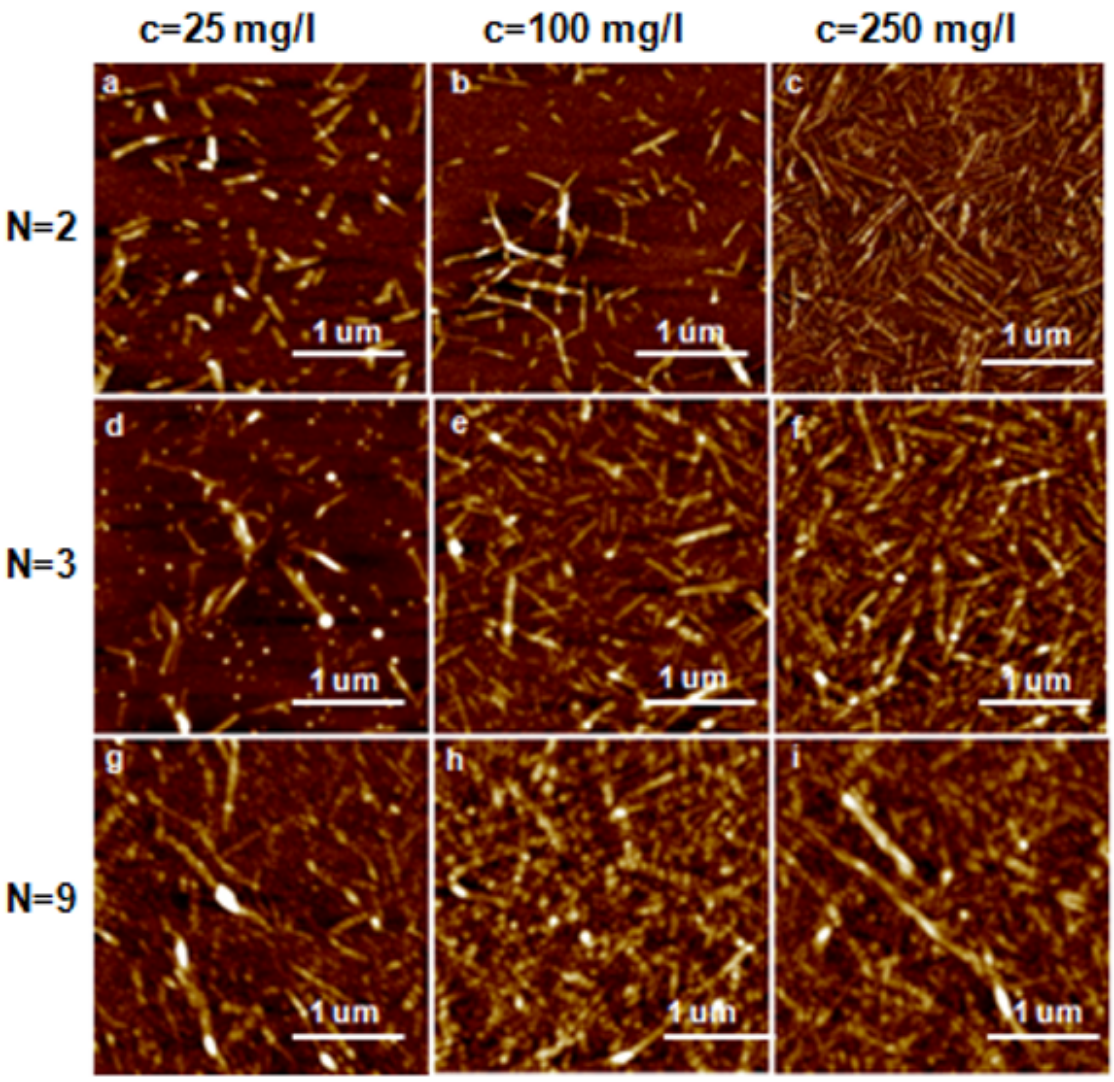

Figure 4

AFM height images of the hybrid samples. The coating layer number (N) and the concentration (c) are denoted for every sample.

Figure 5

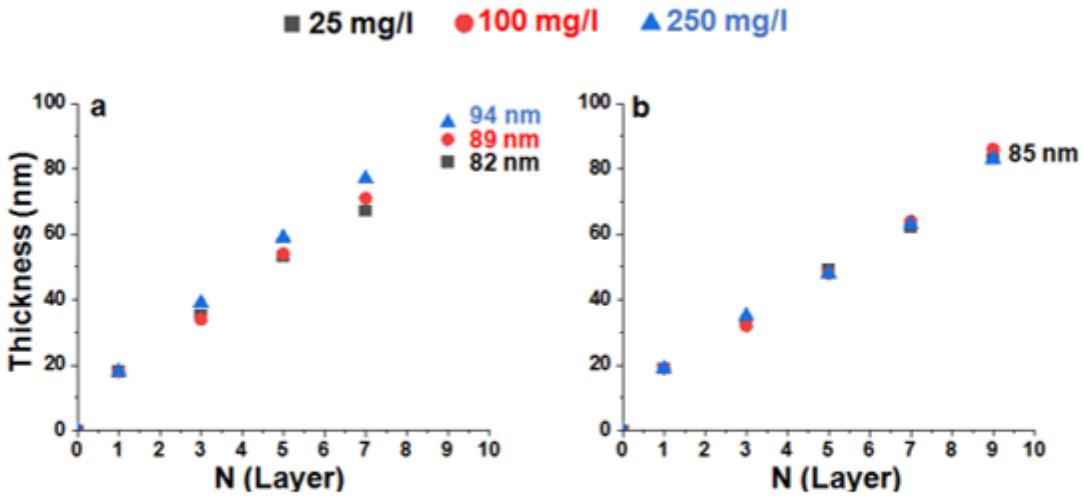

Figure 5

Thickness values of the hybrid samples extracted from (a) Ellipsometry and (b) XRR characterization for all the ZnO/CNC hybrids

Figure 6

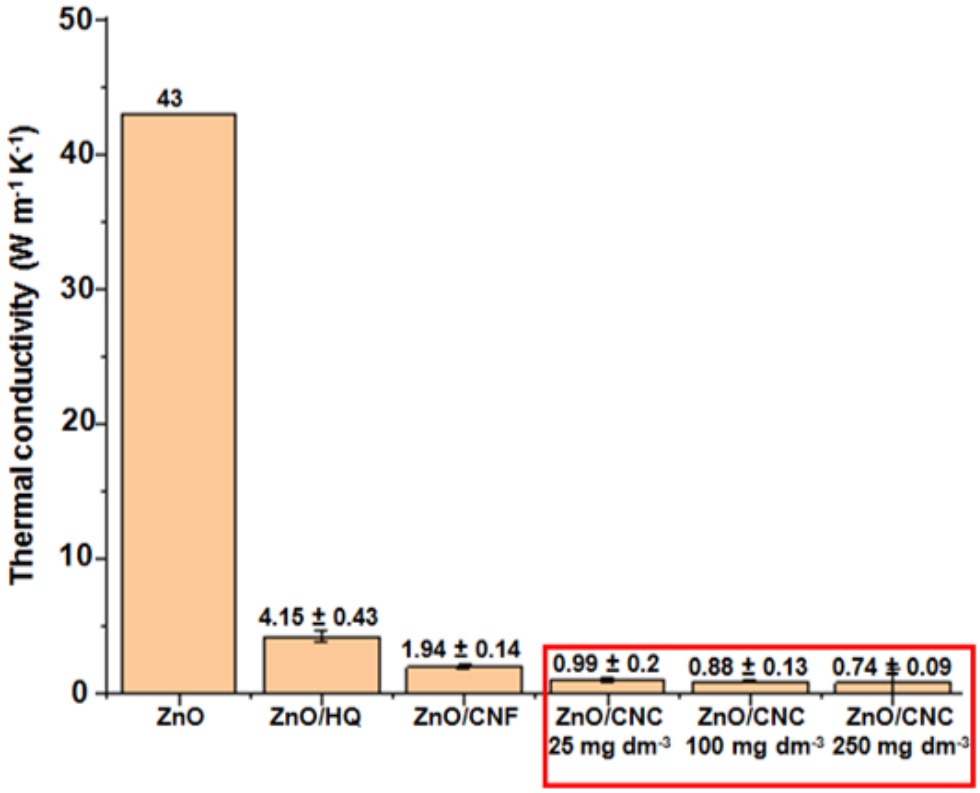

Figure 6

Thermal conductivity values measured for the ZnO/CNC, N=9 hybrid samples (red frame) compared with results of previous studies (Tynell et al. 2014; Jin et al. 2017; Alvarez-Quintana et al. 2010).

Supplementary Files

This is a list of supplementary files associated with this preprint. Click to download.

- SupplementaryInformationfinal.pdf